LAWRENCE
LIVERMORE
NATIONAL
LABORATORY

LLNL-JRNL-414595

Thermal transport in CO2 laser irradiated fused silica: in situ measurements and analysis

S. T. Yang, M. J. Matthews, S. Elhadj, V. G. Draggoo, S. E. Bisson

July 10, 2009

Journal of Applied Physics

Disclaimer

Thermal transport in CO_2 laser irradiated fused silica: in situ measurements and analysis

Steven T. Yang[1], Manyalibo J. Matthews[1], Selim Elhadj[1,*], Vaughn G. Draggoo[1] and Scott E. Bisson[2]

[1]Lawrence Livermore National Laboratory, Livermore, California, 94550, USA

[2]Sandia National Laboratory, Livermore, California, 94550, USA

ABSTRACT

In situ spatial and temporal temperature measurements of pristine fused silica surfaces heated with a 10.6 μm CO_2 laser were obtained using an infrared radiation thermometer based on a Mercury Cadmium Telluride (MCT) camera. Laser spot sizes ranged from 250 μm to 1000 μm diameter with peak axial irradiance levels of 0.13 to 16 kW/cm^2. For temperatures below 2800K, the measured steady-state surface temperature is observed to rise linearly with both increasing beam size and incident laser irradiance. The effective thermal conductivity estimated over this range was approximately 2W/mK, in good agreement with classical calculations based on phonon heat capacities. Similarly, time-dependent temperature measurements up to 2000K yielded thermal diffusivity values which were close to reported values of 7×10^{-7} m^2/s. Above ~2800K, the fused silica surface temperature asymptotically approaches 3100K as laser power is further increased, consistent with the onset of evaporative heat losses near the silica boiling point. These results show that in the laser heating regime studied here, the T^3 temperature dependent thermal conductivity due to radiation transport can be neglected, but at temperatures above 2800K heat transport due to evaporation must be considered. The thermal transport in fused silica up to 2800K, over a range of conditions, can then be adequately described by a linear diffusive heat equation assuming constant thermal properties.

*Author to whom correspondence should be addressed. Electronic mail: elhadj2@llnl.gov

I. INTRODUCTION

Knowledge of the spatially-dependent thermal history of a heated material is fundamental to understanding and controlling laser machining processes. In particular, the nonlinear dependence of ablation rate[1], thermocapillary forces[2] and residual stress[3,4] on the material thermal history requires sensitive tuning of laser parameters to achieve optimal processing. Furthermore, the spatial gradients in surface temperature associated with laser heating can lead to spatial non-uniformities in the final material morphology unless properly addressed. In principle, temperature distribution within the material under laser heating can be calculated by solving the time-dependent heat flow equation. In practice, owing to uncertainty associated with the relevant material thermal properties at high temperatures, direct temperature measurement is needed to validate temperature computational models and to determine the dominant heat transport mechanisms in the laser processing regime of interest. In particular, the contribution from radiative losses and a T^3 dependence of the thermal conductivity is not clear in the case of laser heated silica.

Few direct temperature measurements of high spatial and temporal resolution have been performed on laser heated silica. Previous studies have involved contact and non-contact techniques of measurements. Examples of contact methods include application of a *T*-sensitive phosphor coating[5] or absorptive layer,[6] or deposition of a Pt resistance-thermometer.[7] These contact methods can interfere with the heating process and are often impractical. Non-contact techniques, such as measuring Plank radiation emission or probing the Raman spectrum, are attractive alternatives for measuring temperature in-situ since they can provide spatial and temporal resolution without interfering with the heating process.[8,9] However, previous studies of laser heating using non-contact methods were limited in the spatial[10] or temporal resolution achieved.[11]. Often, the interpretation of the results became problematic when measuring emitted IR radiation in part of the spectrum where silica is semi-transparent.[12-14]

The above limitations encountered in previous studies on laser heated silica can be avoided with the use of a LN-cooled, high responsivity thermal camera coupled with a narrow band optical filter from which 2-D temperature maps at video frame rates can be derived. The focus of this study is on silica because it is a technologically important optical material that is often subject to laser heat treatment for polishing,[13,14] damage mitigation,[15] reshaping,[16] and for conditioning.[17] Our results show that under a wide range of laser operating conditions, simple linear approximations to the heat equation, using constant effective thermal parameters derived by measurement, are sufficient to analyze and describe the temperature spatial and temporal profiles. For 10.6 μm heating of fused silica, radiation transport was thought to cause a marked increase in the effective thermal conductivity at elevated temperature.[4] However, our results show conclusively that this is not the case, at least up to the boiling point of silica. An accurate description of the temperature field is possible without invoking full scale solutions that include all, or part of the non-linear material properties,[18] radiation transport,[19] evaporative cooling,[4] and convection.[20] Limits to this linear approximation will be discussed. The results of this analysis can, in principle, be used to predict the transformation of a broad range of laser heated materials, within the range of irradiance levels for which the linear approximation applies.

II. Infrared radiation thermometry

i) Design and setup

Deriving surface temperatures from measurements of Plank radiation requires careful selection of the detection wavelength, λ_d. For 10.6 μm laser heating of fused silica, an absorption length of less than 40μm leads to a large axial temperature gradient extending a few hundred microns beneath the surface. Detecting Plank radiation in the near IR, where fused silica is semi-transparent, would result in the sampling of thermal radiation from the surface as well as the bulk, requiring a-priori knowledge of the temperature z-dependence to deduce the temperature at the surface.[21] In contrast, detecting Plank radiation at or near the fused silica absorption peak in the long-wave IR range can limit the collection of radiation to within a few hundred nm of the surface where near isothermal conditions exist.[22] Therefore, detection at $\lambda_d \approx 9$ μm wavelength was chosen in this study to coincide with the peak in the restrahl band for fused silica. At this wavelength absorption depths are on the order of a few hundred nanometers,[23] a distance over which the steady-state temperature varies by only a few degrees when laser energy is deposited within a few micrometers of the surface.[24]. Additionally, owing to the rapidly varying emissivity near the 9 μm absorption peak, a single narrow band pass filter centered at 8.9 μm with a band-pass of 0.1 μm was used to limit detection to a single monochromatic band.

Detection of long wave IR radiation was achieved using a liquid nitrogen cooled Mercury Cadmium Telluride (MCT) camera capable of detecting radiation within the 2 to 12 μm range. The MCT camera uses a 256×256 element focal plane array with 40 μm square pixel. Thermal background from the surroundings was removed with the 8.9 μm centered bandpass filter by including the filter as part of the cold shield installed in front of the focal plane array. The MCT camera was run at a maximum speed of 32.8 frames per second, yielding a temporal resolution capability of 30.5 millisecond. The analog output of the focal plane array is converted into 14-bit digital output from the camera.

As shown in **Fig. 1**, a 10.6 μm laser (Synrad firestar V20), with a maximum output power of 20 watts and power stability of ±5%, is used for heating the fused silica sample. The laser beam is collimated with a pair of lenses, and passed through a variable magnification afocal telescope to a 10” focal length final focusing lens. By varying the magnification of the afocal telescope, the collimated beam size at the entrance to the final focusing lens could be adjusted so that the laser spot size on the fused silica surface was varied between 250 μm and 1000 μm without changing the focal location. An un-coated ZnSe wedged plate, inserted before the final focusing lens, is oriented at Brewster’s angle (67.4°) to pass the p-polarized 10.6 μm laser light while reflecting 50% of the ‘S’ polarized fraction of the black body emission collected from the heated surface by the final focusing lens. Since the black body emission is un-polarized, only a quarter of the emitted black body radiation collected is sent to the thermal camera. The final focusing lens collects blackbody emission up to an angle of $\pm 6^{o}$ relative to sample normal. Over this narrow angular range, fused silica emissivity varies less than 2% over the emission angle.[22] Imaging of the fused silica surface was achieved with a second 10” focal length ZnSe lens used in conjunction with the 10” focal length final focusing lens to form a 1:1 image of the heated spot on the camera, resulting in 10mm×10mm field of view. Given a f/# of 5 for the thermal camera imaging setup, a lateral

spatial resolution of better than 200 μm can be achieved. Average laser power was measured at the sample plane before measurements using a standard IR optical power meter. Laser beam size was measured using a beam profiler (Pyrocam III, Spiricon, Logan, UT). All experimental beam sizes reported here correspond to $1/e^2$ beam diameter at the sample plane. The duration of the laser exposure was fixed at 5 sec and the total camera acquisition time was nominally 10 sec to capture the temperature evolution after laser turn on. The fused silica parts used in this study were UV-grade Type III (800-1200ppm OH) glass 7980 from Corning (NY, USA). All samples are 51 mm in diameter and 10 mm thick prepared with an optical polish. All experiments were conducted in ambient air.

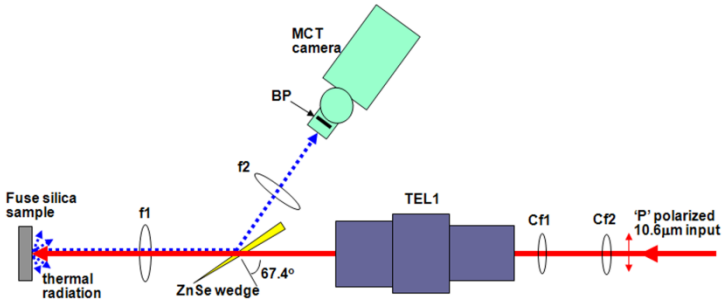

FIG. 1. Schematic of optical system and MCT camera used for in-situ surface temperature measurement of CO_2 laser heated samples. The red solid line marks the CO_2 laser beam path; the blue dotted line indicates the emitted thermal emission. Cf1, Cf2, f1 and f2 are ZnSe lenses; TEL1 is a telescope with variable magnification; BP is the narrow-band bandpass cold filter centered at 8.9 μm placed immediately in front of the MCT camera.

ii) Deriving surface temperature from thermal emission

The infrared radiation thermometer was calibrated against a cavity black body source to derive the surface temperature based on the detected single wavelength band thermal emission. For this purpose, a commercial cavity-type blackbody source (Graseby IR Systems, FL, USA) with temperature that can be set from 290 to 1473K is used. For calibrating the thermal camera, the blackbody source is placed at the location of the fused silica sample, with the thermal camera imaging the aperture of the black body source. The detected thermal flux then includes transmission loss through the intervening optics and can be fitted to the following equation:

$$C = A + B \cdot \varepsilon(T) \cdot \frac{c_1}{\lambda^5 \exp(\frac{c_2}{\lambda T}) - 1} \cdot \Delta\lambda \quad , \qquad \textbf{(1)}$$

Where $\varepsilon(T)$ is the temperature dependent normal spectral emissivity, T is the blackbody temperature in Kelvin, $\lambda=\lambda_d$ is the detection wavelength, $\Delta\lambda$ is the bandpass filter full-width-half-maximum, and $C_{1,2}$ are the first and second radiation constants[9]; A and B are parameters determined by least square fit to **Eq. (1)** as a function of temperature.

As shown in **Fig. 2A**, the blackbody calibration data was well fitted by **Eq. (1)**, up to the maximum blackbody temperature of 1473K. The linearity of the camera was verified up to a peak count of 9000, which ensures that the calibration holds throughout the temperature range studied. The thermal camera noise count yields a noise limited temperature resolution of 50 and 1.5K at temperature of 300 and 1500K respectively. From propagation of error analysis of the temperature measurement equation, we estimate the relative uncertainty of absolute temperature measurement error to be ~3%. At a temperature of 2000 K, this error corresponds to a measurement uncertainty of ±60 degrees K.

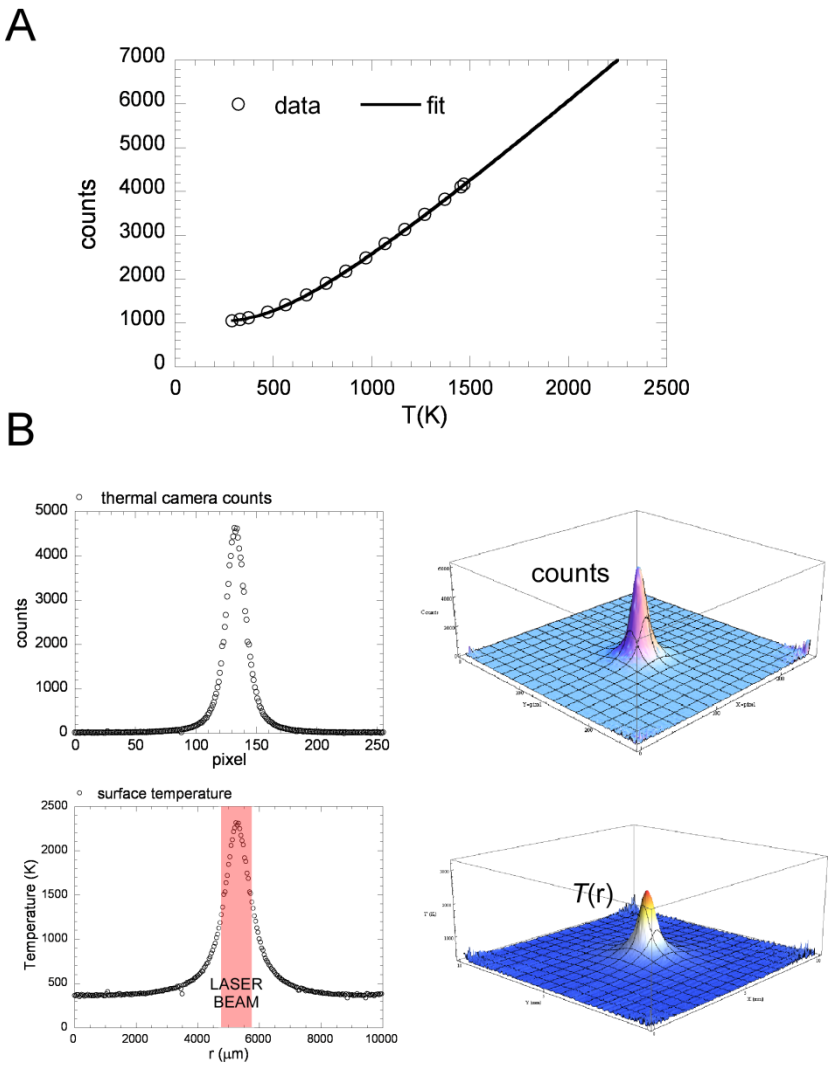

FIG. 2. (A) Calibration data of the MCT camera counts against the known blackbody source cavity temperature. The fit is based on Planck's law for blackbody radiation, **Eq. (1)**. This data is used to relate the measured pixel array counts to the flux incident at the detector array to derive 2D experimental temperature profiles as illustrated in (B). The thermal camera pixel counts and corresponding temperature spatial distribution shown here are for a CO_2 laser heated silica surface (D=1000μm, 6.5W, 5 sec exposure).

Once the thermal camera has been calibrated using the blackbody source, thermal counts measured during laser heating can be converted into temperature by inverting **Eq. (1)**, taking into account the temperature dependent emissivity of fused silica at 8.9 μm.[25] Shown in **Fig. 2B** is an

example of a single frame of thermal camera output, captured during laser heating, plotted in counts along with the derived temperature distribution. As expected for heating with a Gaussian laser beam, the temperature profile follows a roughly Bessel function-weighted Gaussian shape.

iii) Comparison of thermal camera measurements with temperature sensitive lacquers

As an independent check of measurement accuracy, temperatures derived from the MCT camera measurement were compared with results of measurements using temperature-sensitive lacquers. A subset of the fused silica parts were prepared with temperature sensitive lacquers with melting point ranging from 575K to 1089K (Omega Engineering Inc., CT, USA). Droplets of the lacquer were applied directly to the sample surface close to the location of laser heating, but far enough away to avoid direct exposure to the laser light. When the heating starts, an expanding region of the lacquer melts as the underlying surface temperature reaches and exceeds the lacquer's calibrated melting point. When the laser heating stops, the melted region of lacquer re-crystallizes, permanently marking the area where the surface temperature is equal to or greater than the rated melting point as delineated in **Fig. 3**. The boundary of the clear region marks the location where the surface temperature just reached the lacquer melting point. A temperature profile can be reconstructed from application of lacquers with different melting points, and by measuring the distance from the center of the laser heated spot to the boundary (**Fig. 3**). This lacquer derived profile is compared to that obtained from a single frame of the thermal camera captured for the same beam parameters at steady state. The good agreement between these measurements is used to validate the temperature measurement procedure using the MCT thermal camera.

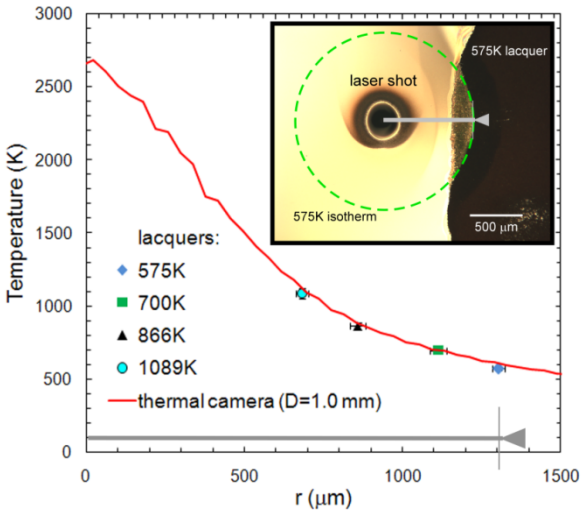

FIG. 3. Comparison of the measured steady state surface temperature spatial profile obtained using the 9 μm bandpass MCT thermal camera with the profile reconstructed from temperature sensitive lacquers. Legend indicates lacquers temperature ratings and beam size.

III. RESULTS AND DISCUSSION: TEMPERATURE ANALYSIS

i) Temperature modeling of laser heated surface

The temperature distribution *T(r,z,t)* for axisymmetric laser heating of a homogeneous medium can be obtained by solving the 2-D heat flow equation:

$$\rho C_p \frac{\partial T}{\partial t} - \nabla(k\nabla T) = Q\,, \qquad \textbf{(2)}$$

where ρ is the density, C_p is the specific heat, k is the thermal conductivity and Q is the heat source term. In the case of volumetric heating with a Gaussian laser beam, the heat term is expressed as $Q(r, z)=(\alpha I)\exp(-\alpha z)\exp(-(r/a^2))$, where $I= P/\pi a^2$ is the absorbed laser irradiance, α is the material absorption coefficient, a is the 1/e beam radius, r and z are the radial and axial coordinates inside the bulk of the heated material.

The full heat transport equation can be solved numerically taking into account radiative heat loss, surface heat loss through convection, and temperature dependent material properties. This approach, however, is computationally intensive and does not readily yield physical insights into laser energy deposition and transport processes. An alternate approach is to neglect radiative and surface heat loss and to assume that the thermal properties are constant over the temperature range of interest. Using this linear diffusive approximation, the heat equation can be readily solved numerically using the Green's function method to express T as an integral,[26]

$$T(r,z,t) = \frac{I}{4k}\int_0^{\sqrt{4Dt}} \frac{\alpha l}{l^2/a^2+1} Exp\left(-\frac{r^2}{a^2+l^2}+\frac{\alpha^2 l^2}{4}\right)\left(Exp(\alpha z)Erfc\left(\frac{\alpha l}{2}+\frac{z}{l}\right)+Exp(-\alpha z)Erfc\left(\frac{\alpha l}{2}-\frac{z}{l}\right)\right)dl \qquad \textbf{(3)}$$

and integrating over $l = \sqrt{4Dt}$, where $D = k/\rho C_p$ is the thermal diffusivity. While a, P, α and ρC_p are either known from experiment or literature, k and D can be influenced by non-thermal transport mechanisms such as radiation and evaporation. Therefore, we use an analytic on-axis approximation to **Eq. (3)** to extract the *effective* thermal conductivity (k_e) and diffusivity (D_e) from experiment in the limit of $a\alpha\rightarrow\infty$ (surface source), and then compare the full solution to the entire surface temperature map over finite $a\alpha$. In the surface source limit, the on-axis surface temperature rise as a function of absorbed laser irradiance can be expressed as

$$\Delta T(0,0,\infty) = \frac{aI\sqrt{\pi}}{2k_e} \qquad \textbf{(4)}$$

in the steady state condition ($t>>a^2/4D$), and as

$$\Delta T(0,0,t) = \frac{aI}{\sqrt{\pi}k_e}\tan^{-1}\left(\sqrt{\frac{4D_e t}{a^2}}\right) \qquad \textbf{(5)}$$

under transient conditions. Thus in the steady state limit, the peak surface temperature at the beam center is proportional to the incident laser power and inversely proportional to thermal conductivity, while the temperature evolution time constant goes as roughly the square root of the thermal diffusivity. For larger beam radii (≈1mm), the assumption of surface confined heating is justified for 10.6 μm laser heating of silica because the absorption length α^{-1}<40 μm is much smaller than the 1/e radius *a*.[27]

ii) Steady state peak surface temperature

Predictions based on the temperature solutions presented above were tested against a series of temperature measurements with different laser heating beam sizes and power levels ranging from 0.4 to 12 W in a 5 sec flat-in-time pulse. Measured peak steady state surface temperatures for five beam sizes ranging from 250 to 1000 μm are summarized in **Fig. 4**. Peak temperatures were obtained at the end of the 5 second laser pulse before laser turn off when the temperature has reached steady-state (the thermal diffusion time for all beam sizes were <1s). At the center of the beam, the maximum temperature achieved for a given beam power is observed to remain linear up to ~2800K for all beam sizes, scaling inversely with beam size as per **Eq. (4)**. Above 2800K, the peak temperature approaches a limiting value of 3100K, independent of beam radius. Subsequent visual inspection and profilometry scans (data not shown) confirmed that craters were generated at surface sites where temperatures were in excess of 2800-3000K.

The solid lines in **Fig. 4A** represent least square fits of the peak temperatures vs. laser power based on **Eq. (4)** with thermal conductivity as the single fitting parameter. The effective thermal conductivity, k_e, obtained varied from 2 to 3 W/mK, which is within the range of published measurements, depending on the type of glass and measurement method used.[29] For incident power levels below evaporation, the linearity of the peak temperature with laser power and the good fit of the temperature measurements to **Eq. (4)** with constant thermal conductivity (**Fig. 4A**), suggests that radiation transport -often approximated as T^3-dependent- is not significant in this regime.[30,31] However, because the approximation used to derive **Eqs. (4)** and **(5)** fail in the limit of small beam size ($a\alpha \rightarrow 0$), higher conductivity values thus derived might incorrectly suggest some additional heat loss mechanisms. Therefore, to illustrate and determine directly the dependence of *k* on temperature, large spot (1000 μm) data from **Fig. 4A** was used to estimate the experimental *k* values, which were then compared with published and calculated values (**Fig. 4B**). The black solid line is the calculated classical value for phonon conduction as given by $k(T)=\rho C_p(T)vl/3$, where v=4200m/s is the mean phonon velocity, l=0.56nm is the phonon mean free path, and $C_p(T)$ is the temperature dependent heat capacity from Smyth *et al*.[32] The blue line, which agrees with the calculated classical values, represents the measured *k* from Wray *et al,* where radiation was carefully eliminated in the experiment.[33] In contrast, the red line represents measurements of *k* by Kingery *et al* in which radiation losses were not prevented, and were shown to be the dominant transport mechanism (scaling roughly as T^3) above 700K.[34] Experimental *k* values derived in this study follow more closely the phonon-only measurements and calculations, and diverge from Kingery *et al* measurements, suggesting a lack of significant radiation contribution to the heat transport.

This conclusion is further supported by the observation that if radiation transport effects were significant, the expected T^4 dependence in radiative heat loss would cause the effective thermal conductivity to increase with temperature, resulting in a clamping of the *T* vs. *P* curves in **Fig. 5A**. Instead, such behavior is not observed until a temperature of ~3000K is reached, which corresponds to the boiling of silica.[34] As indicated earlier, visual inspection of sites that were heated to temperatures above 2800K revealed cratering thus indicating significant mass and heat loss due to evaporated material. Therefore, we attribute this apparent temperature clamping to a sharp increase in the evaporation rate that dissipates laser power through the latent heat of vaporization,[35] rather than through radiation losses. Nonetheless, influence from radiation at higher temperatures still cannot be excluded, and further work is necessary to quantify the relative contributions of both evaporation and radiation to heat dissipation during laser heating.

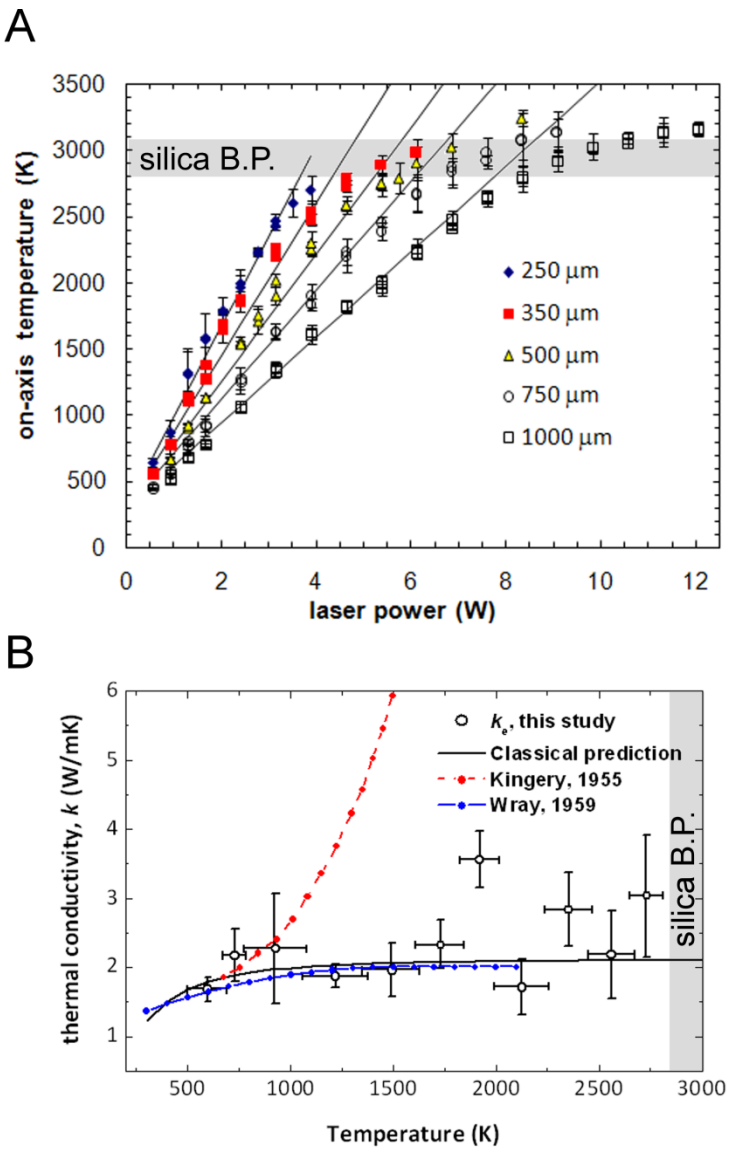

FIG. 4. (A) Measured on-axis steady state surface temperature as a function of laser power and beam size (symbols). The solid lines represent least-squares fits to **Eq. (3)**. (B) Several measurements of 1000 μm beam diameter data were averaged and used to derive an effective thermal conductivity, $k_e(T)$ (open circles), which is compared to both published and calculated values as described in the text.

iii) Measurement of peak surface temperature temporal profile

In addition to extracting steady state thermal measurements, the recorded thermal camera captures time-dependent temperature profiles of the laser heated surface with a 30ms sampling rate and 200μs integration times. **Figure 5** shows the measured time dependent rise of the on-axis surface temperature, $T(0,0,t)$, due to laser heating for a beam diameter of 1000 μm and for power levels ranging from 0.68W to 5.6W**.**

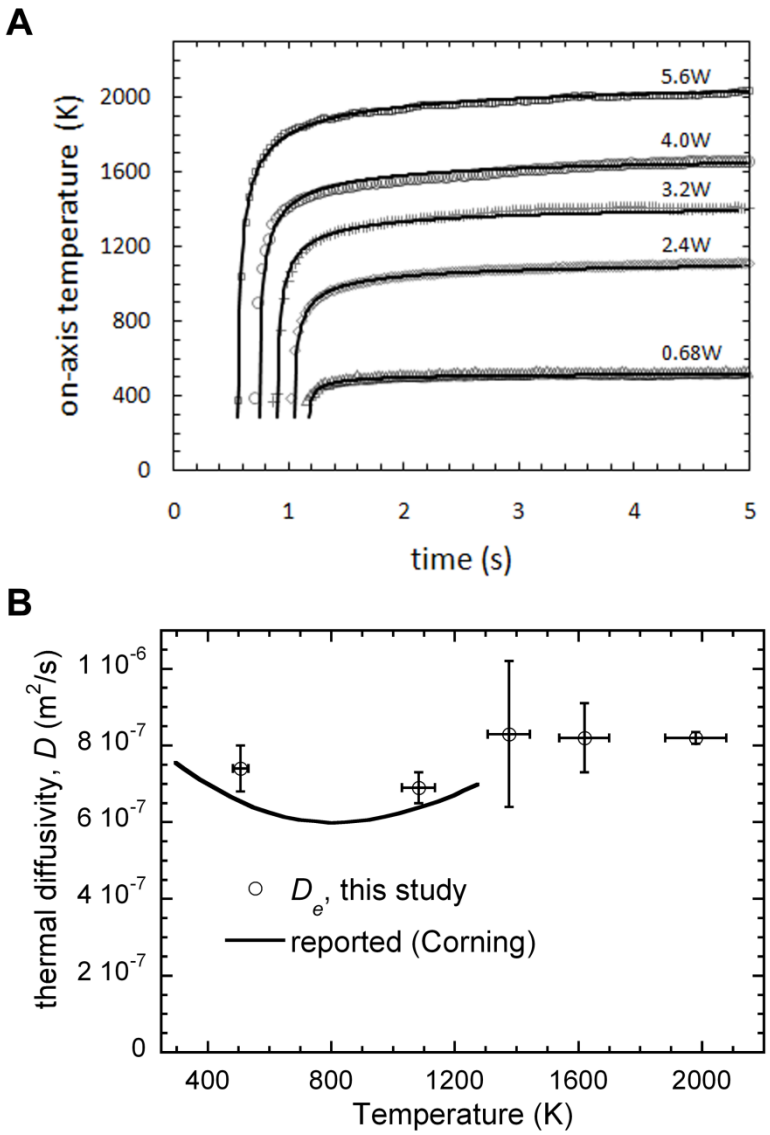

FIG. 5. (A) Transient on-axis temperature measured with the MCT camera. A series of shots at the indicated beam powers with beam diameter of 1000 μm, were fitted with **Eq. (5)** to yield (B) the apparent thermal diffusivity for the corresponding beam powers used. For comparison, the solid curve corresponds to the manufacturer's bulk reported values (Corning, Inc).

Fitting **Eq. (5)** to the measured temporal profile and using a value of 2 W/mK for k_e obtained from section III-ii, we extracted effective thermal diffusivity values for a range of incident laser powers and temperatures. The fitting range was limited to the highest 10% of the temperature curve to derive more narrowly defined temperature-dependent D_e values, as indicated by the horizontal error bars in **Fig. 5B**. As shown in the figure, the effective thermal diffusivity values agree well with reported values.[36] In the phonon-only limit for heat conduction where both phonon mean free path and velocities are temperature independent, the conductivity scales with heat capacity, yielding a nearly temperature independent diffusivity. However, as with most reported values of diffusivity, the Corning measurements cited here were performed under conditions similar to those used in Kingery *et al* where radiation can contribute. Within the error bars of our measurement, we observed no significant increase of diffusivity with temperature.

iv) Transient and Steady state surface temperature spatial profiles

Experimental transient and steady state surface temperature spatial profiles for samples exposed to a 1 mm diameter heating beam are plotted in **Fig. 6**. Temperature profiles calculated using **Eq. (3)**, based on the effective thermal properties k_e = 2 W/m K and D_e=7.3E-7 m^2/s derived from on-axis temperature measurements, are plotted for comparison. Fig. 6a) shows the evolution of spatial temperature profiles at t=0.012, 0.152, 0.52 and 5 seconds after turn-on of a 3.5 watt laser beam. Early in the heating process (t=0.012s), only the area within one beam diameter shows a temperature rise. As time progresses, the peak surface temperature quickly approaches steady state value, rising by 1200 degrees within the first 0.5 seconds, followed by a slower rise of 150 degrees over the next 4.5 seconds . During this time, the heat diffuses away from the center of the beam to the wings by conduction so that at the end of the 5 second laser exposure, the heat has spread to three times the beam diameter. Comparing the measured data against calculation using the effective thermal parameters, there is good agreement at all time slices.

Fig. 6b) shows the steady state spatial temperature profiles of fused silica surface when heated at four power levels ranging from 1.29 to 5.75 watts. The steady state temperature profiles are taken at the end of the 5 second long laser exposure. At these power levels, for which the peak temperature remained below the fused silica boiling point, the measured temperature profiles are in fair agreement with prediction everywhere. The residual small discrepancy at the wings of the spatial profiles may be due to temperature dependence of the thermal conductivity. Nonetheless, the good overall agreement between measured and calculated spatial profiles, in both the transient and steady state regimes, again underscores the validity of linear diffusive and temperature independent thermal constant approximations.

A

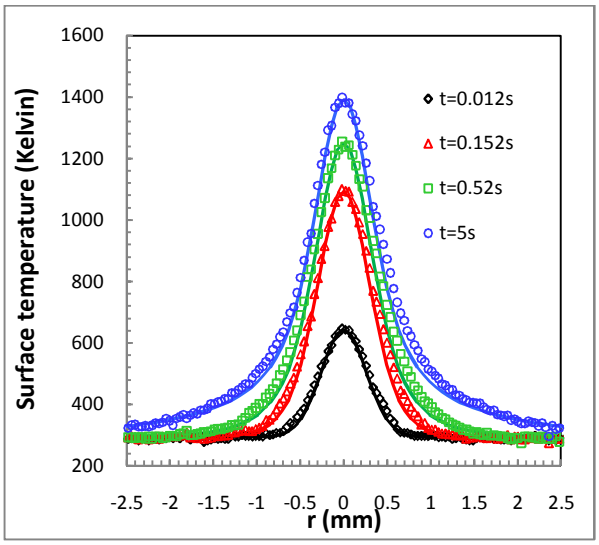

B

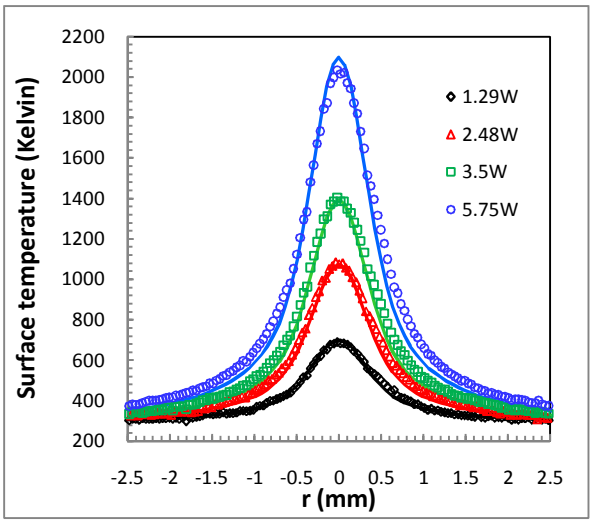

FIG. 6. Transient and steady state spatial temperature profiles of fused silica surface irradiated with 1mm diameter beam. A) Transient temperature profiles at the designated times with incident laser power of 3.5 watts. B) Steady state temperature profiles when irradiated at the indicated power levels. The data points denote experimental data while the solid lines are calculated based on **Eq. (3)** Using effective thermal properties determined from least-squares fits to on-axis temperature measurements as described in the text.

IV. CONCLUSIONS

Surface temperatures of fused silica heated up to ~3100K with a CO_2 laser (10.6 μm) were measured *in situ* with an accuracy of ~3% using a MCT camera. Measured steady state peak temperature is seen to rise linearly with laser power for temperatures below 2800K. Above 2800K, the silica peak temperature rises sub-linearly and asymptotically approaches 3100K with increasing laser

power, consistent with increasing evaporative heat loss near the boiling point of silica. Dynamically, the peak surface temperature rises rapidly at laser start, reaching steady state over times consistent with independently measured thermal diffusivities. Spatially, the temperature profile exhibits a sharp peak at laser beam center, with significant heat diffusion out to a few beam diameters. The temperature-dependent thermal conductivity of silica derived in this study agrees with phonon-only calculations and non-radiative measurements reported in earlier studies. These results show that, below the onset of significant evaporation at $T \sim 2800$K, radiation transport does not play an important role in the time-dependent surface temperature distribution of laser heated silica. Thus, the simple linear heat diffusion equation can be used to accurately describe the temperature of laser heated silica over a broad range of conditions.

ACKNOWLEDGMENTS

The authors would like to acknowledge Drs. James Stolken, Jeffrey Bude and Michael Feit for stimulating discussions and insights into evaluating heat transport mechanisms. Thanks are due to Dr. Michael A. Johnson for gracious use of laboratory equipment and suggesting use of thermal lacquer.

This work performed under the auspices of the U.S. Department of Energy by Lawrence Livermore National Laboratory under Contract DE-AC52-07NA27344.

REFERENCES

[1]E. Mendez, K. M. Nowak, H. J. Baker, F. J. Villarreal, and D. R. Hall, Applied Optics 45, 5358-5367 (2006).
[2]T. R. Anthony and H. E. Cline, Journal of Applied Physics 48, 3888-3894 (1977).
[3]F. Dahmani, A. W. Schmid, J. C. Lambropoulos, and S. Burns, Applied Optics 37, 7772-7784 (1998).
[4]A. M. Rubenchik and M. D. Feit, in *Laser-Induced Damage in Optical Matls. 2002/7th Intl. Wkshp. on Laser Beam & Optics Characterization* (SPIE, 2003).
[5]R. I. Altkorn, J. C. Andreshak, and A. Gupta, Applied Physics a-Materials Science & Processing 48, 273-276 (1989).
[6]B. Adams, A. Mayur, A. Hunter, and R. Ramanujam, 13th IEEE International Conference on Advanced Thermal Processing of Semiconductors - RTP 2005, 105-109 292 (2005).
[7]R. Zenobi, J. H. Hahn, and R. N. Zare, Chemical Physics Letters 150, 361-365 (1988).
[8]J. Kolzer, E. Oesterschulze, and G. Deboy, Microelectronic Engineering 31, 251-270 (1996).
[9]Z. M. Zhang, in *Annual Review of Heat Transfer Online*; *Vol. 11*, edited by V. Prasad, Y. Jaluria, and G. Chen (Begell House, Redding, Connecticut, 2000), p. 351-411.
[10]S. C. Chen and C. P. Grigoropoulos, Applied Physics Letters 71, 3191-3193 (1997).
[11]J. B. Cui, K. Amtmann, J. Ristein, and L. Ley, Journal of Applied Physics 83, 7929-7933 (1998).
[12]C. Buerhop and R. Weissmann, Glass Technology 37, 69-73 (1996).
[13]F. Laguarta, N. Lupon, and J. Armengol, Applied Optics 33, 6508-6513 (1994).
[14]F. Vega, N. Lupon, J. A. Cebrian, and F. Laguarta, Optical Engineering 37, 272-279 (1998).
[15]I. L. Bass, V. G. Draggoo, G. M. Guss, R. P. Hackel, and M. A. Norton, High-Power Laser Ablation VI, Pts 1 and 2 6261, A2612-A2612 856 (2006).
[16]M. J. Matthews, I. L. Bass, G. M. Guss, C. C. Widmayer, and F. L. Ravizza, Laser-Induced Damage in Optical Materials: 2007 6720, A7200-A7200 359 (2008).
[17]R. M. Brusasco, B. M. Penetrante, J. E. Peterson, S. M. Maricle, and J. A. Menapace, Laser-Induced Damage in Optical Materials: 2001 Proceedings 4679, 48-55 452 (2002).
[18]M. Lax, Applied Physics Letters 33, 786-788 (1978).
[19]E. W. Larsen, G. Thommes, and A. Klar, Siam Journal on Applied Mathematics 64, 565-582 (2003).
[20]J. Mazumder, Optical Engineering 30, 1208-1219 (1991).
[21]R. Van Laethem, L. Leger, M. Boffe, and E. Plumat, Journal of the American Ceramic Society 44, 321-332 (1961).
[22]R. Gardon, Journal of the American Ceramic Society 39, 278-287 (1956).
[23]R. Kitamura, L. Pilon, and M. Jonasz, Applied Optics 46, 8118-8133 (2007).
[24]A. D. Mclachlan and F. P. Meyer, Applied Optics 26, 1728-1731 (1987).
[25]O. Rozenbaum, D. D. Meneses, Y. Auger, S. Chermanne, and P. Echegut, Review of Scientific Instruments 70, 4020-4025 (1999).
[26]H. S. Carslaw and J. C. Jaeger, *Conduction of Heat in Solids*, 2nd ed. (OXFORD university press, Great Clarendon, 2000).
[27]M. Lax, Journal of Applied Physics 48, 3919-3924 (1977).
[28]Y. S. Touloukian, R. W. Powel, C. Y. Ho, and P. G. Klemens, in *Thermophysical Properties of Matter*; *Vol. 2*, edited by Y. S. Touloukian and C. Y. Ho (IFIPlenum, New York, 1970), p. 183-193.
[29]H. Charnock, Journal of the American Ceramic Society 44, 313-317 (1961).
[30]W. D. Kingery, Journal of the American Ceramic Society 44, 302-304 (1961).
[31]H. T. Smyth, H. S. Skogen, and W. B. Harsell, Journal of the American Ceramic Society 36, 327-328 (1953).
[32]K. L. Wray and T. J. Connolly, Journal of Applied Physics 30, 1702-1705 (1959).
[33]W. D. Kingery, Journal of the American Ceramic Society 38, 251-255 (1955).
[34]H. L. Schick, Chemical Reviews 60, 331-362 (1960).

[35]R. Brückner, Journal of Non-Crystalline Solids 5, 123-175 (1970).
[36]Corning, edited by I. Matthews (2008).